^{135}La as an Auger-electron emitter for targeted internal radiotherapy

J. Fonslet[1], B.Q. Lee[2,3], T.A. Tran[4], M. Siragusa[1], M. Jensen[1], T. Kibédi[3], A.E. Stuchbery[3], G.W. Severin[1,5,6*]

[1]*Hevesy Laboratory, Center for Nuclear Technologies, Technical University of Denmark, Roskilde, Denmark*

[2]*Department of Oncology, Oxford University, Oxford, United Kingdom*

[3]*Department of Nuclear Physics, Australia National University, Canberra, Australia*

[4]*Lund University Bioimaging Center, Lund University, Lund, Sweden*

[5]*Department of Chemistry, Michigan State University, East Lansing, MI, USA*

[6]*Facility for Rare Isotope Beams, Michigan State University, East Lansing, MI, USA*

Abstract:

Introduction: ^{135}La has favorable nuclear and chemical properties for Auger-based targeted internal radiotherapy. Here we present detailed investigations of the production, emissions, and dosimetry related to ^{135}La therapy.

Methods and Results: ^{135}La was produced by 16.5 MeV proton irradiation of metallic ^{nat}Ba on a medical cyclotron, and was isolated and purified by trap-and-release on weak cation-exchange resin. The average production rate was 407 ± 19 MBq/µA (saturation activity), and the radionuclidic purity was 98% at 20 h post irradiation. Chemical separation recovered > 98 % of the ^{135}La with an effective molar activity of 70 ± 20 GBq/µmol. To better assess cellular and organ dosimetry of this nuclide, we have calculated the X-ray and Auger emission spectra using a Monte Carlo model accounting for effects of multiple vacancies during the Auger cascade. The generated Auger spectrum was used to calculate cellular S-factors.

Conclusion: ^{135}La was produced with high specific activity, reactivity, radionuclidic purity, and yield. The emission spectrum and the dosimetry are favorable for internal radionuclide therapy.

Keywords: lanthanum-135, La-135, radiolanthanide, auger therapy, targeted radionuclide therapy, radionuclide production

* gwseverin@chemistry.msu.edu – corresponding author

Introduction:

The development of targeted internal radiotherapy for cancer and patient specific treatment requires radionuclides with suitable half-lives, chemical properties and emissions. Several nuclides are already in clinical use, notably the beta emitters ^{177}Lu and ^{90}Y [1,2]. In addition, preclinical studies with other lanthanides, especially the terbium isotopes $^{149, 151, 155, 161}$Tb show promise, providing a matched set of isotopes with diagnostic positrons and therapeutic alpha- and beta-particles, as well as Auger electrons [3–6]. The radioactive isotopes of lanthanum are chemically similar to the other lanthanides, and one in particular, ^{135}La has potential as a therapeutic Auger electron emitter.

Auger electron emitters are particularly interesting because they have the capability to deliver radiation dose to individual targeted cells while sparing surrounding tissues. This is in contrast to more commonly-used therapeutic nuclides, like ^{177}Lu and ^{90}Y, which have beta emissions that traverse many cell lengths, with dispersed energy deposition. The very low energy and multiplicity of Auger electrons may prove useful in targeted therapy, especially in the treatment of diffuse and disseminated disease, where other nuclear emissions do not allow adequate dose to the targeted cell due to excessive particle range. Further, there is mounting evidence that the relative biological effectiveness (RBE) of multiple low energy electrons (<10 keV) significantly exceeds that of photons and higher energy beta particles [7]. In some cases the biological effect of absorbed dose from Auger electrons is 2-10 times higher than X-rays of the same energy, meaning that these emissions are more potent in introducing radiation damage to living cells [8–10]. Therefore, coupling Auger emitting radionuclides like ^{135}La with highly specific targeting vectors, particularly cell-nucleus targeting moieties, has potential as a powerful therapeutic tool.

^{135}La decays by electron capture (EC), primarily (>98%) to the ground state of stable ^{135}Ba, with a half-life of 18.9 hour [11] (Figure 1). Following the decay Auger electrons are emitted which are potentially useful for internal radiotherapy. Throughout this paper we use the term “Auger electrons” as designation for all Auger cascade electrons, including the Coster-Kronig and Super-Coster-Kronig electrons. X-rays accompany the Auger cascade with a spectrum sufficient for Single Photon Emission Computed Tomography (SPECT) imaging capabilities. This allows for concurrent SPECT imaging in small animals, facilitating dosimetry calculations in small animal models [12]. In the projected future human use of therapeutic doses, the activity could be high enough to allow whole-body SPECT based on the 480.5 keV gamma emissions.

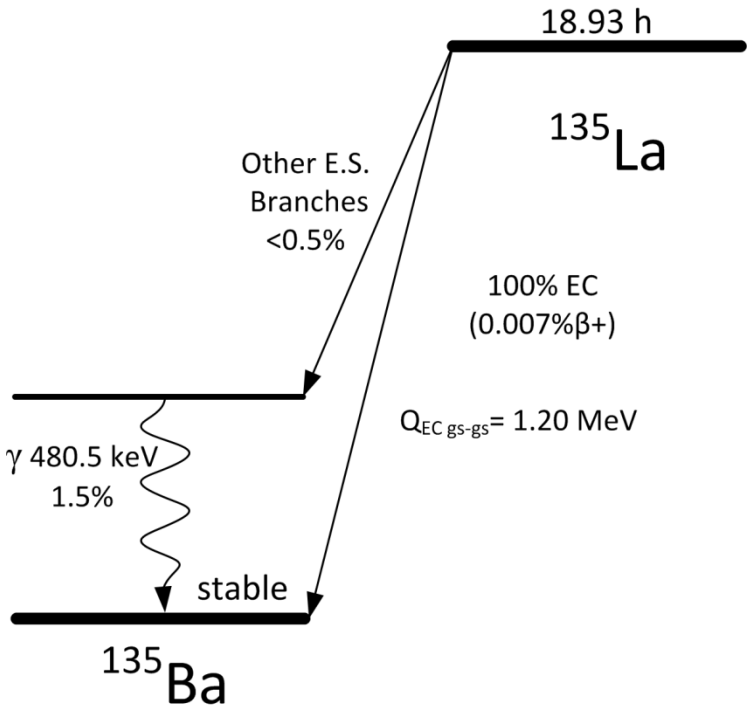

Figure 1 Simplified decay scheme of ^{135}La[11,13].

When considering employing ^{135}La as a radiotherapeutic nuclide, it is necessary to make detailed dose calculations. This is important not only on the organ level, but also on the cellular level, due to the highly localized dose deposition from emitted Auger electrons. In order to get a realistic dose estimate the entire emission spectrum needs to be well understood. The conventionally-used databases (like NuDat 2 [14]) only give a condensed version of the Auger cascade emissions, without addressing the many electrons below 3 keV. Lee et al. recently developed an Auger-cascade model, BrIccEmis, based on a Monte Carlo technique for determining X-ray and Auger emission spectra [15,16]. For the present work, the model was used to obtain detailed radiation spectra from ^{135}La, especially for very low-energy Auger electrons and X-rays. Prescher et al. [17], and Tárkányi et al. [18] determined the production cross-sections for ^{135}La during proton irradiation of ^{nat}Ba at energies ranging from 12-70 MeV. Evident in their data is the fact that ^{135}La is the primary radionuclide with half-life longer than a few minutes produced in the proton-induced reactions on natural barium at energies available on most medical cyclotrons.

In this work, we detail the properties of ^{135}La as a radiotherapeutic nuclide. The practical considerations of production, purification, and radiolabeling are experimentally determined and optimized for the chelator DTPA (diethyeneltriaminepentacetic acid). Additionally, reevaluations of the Auger and X-ray

emission spectra are presented along with a calculation of the cellular *S*-factors and a dosimetry comparison to the commonly used radiotherapeutic isotopes ^{177}Lu and ^{90}Y.

Materials and Methods:

General

All reagents were obtained from Sigma Aldrich and used without further purification unless otherwise noted. All water was 18 MΩ MilliQ-grade (Sartorious). Hydrochloric acid (HCl) solutions were diluted from 37% aq. HCl (Fluka TraceSelect) with water. pH was determined by pH paper (PEHANON 1-12 and 4-9). Gamma spectroscopy was performed on a Princeton Gammatech LGC 5 germanium detector, calibrated using certified ^{133}Ba and ^{152}Eu sources.

Cyclotron Production of ^{135}La from ^{nat}Ba

Chunks of dendritically distilled metallic barium (99.99% trace metal grade) totaling 314-550 mg were pressed with a hydraulic press (20 kN/cm^2) into a 9 mm diameter x 3 mm deep divot in a 28 mm diameter x 5 mm thick silver disc. The barium was immediately covered with either 100 µm aluminum or 25 µm niobium foil to reduce the exposure to atmospheric oxygen, and placed into a target holder supplying direct water cooling to the backside of the silver. A rough schematic of the target and target holder can be seen in a paper by Severin et al. [19]. The target holder was mounted onto a PETtrace cyclotron (PT800 General Electric) and irradiated at 90° (normal) incidence with 16.5 MeV protons at 15 µA for 235-280 min. Owing to the co-production of short-lived ^{134}La ($t_{½}$ = 6.5 min) and ^{136}La ($t_{½}$ = 9.9 min), and slightly longer-lived ^{132}La ($t_{½}$ = 4.5 h) and ^{133}La ($t_{½}$ = 3.9 h), the targets were allowed to decay for 12-24 hours before further handling.

In order to determine the production rates of ^{135}La and the other longer-lived co-produced radioisotopes (^{132}La, ^{133}La and ^{135m}Ba), a single thick target of Ba totaling 472 mg was irradiated at 30 µA for 227 minutes. This target was dissolved 19.8 hours post irradiation in 5 mL 1.2 M HCl, transferred to a plastic vial, and the radionuclidic contents were quantified by gamma spectroscopy.

Purification of ^{135}La

The cover foil was removed and the silver disc mounted in a dissolution chamber allowing the barium to be dissolved with 2 mL 4 M aq. HCl. After complete dissolution of the ^{nat}Ba, the solution was transferred to a vial along with 1-2 mL of water to rinse. Adding the water also served to dissolve any additional white precipitate present after oxidation of Ba in HCl/water. Therefore, concentrated HCl was added to the dissolved target to bring the HCl concentration to 1 M acidity in a final volume of 4 mL. The solution

was then heated at 70 °C for at least 30 min. The pH was adjusted to ~6 with 5 mL HEPES buffer (4-(2-hydroxyethyl)-1-piperazineethanesulfonic acid) (1 M, pH = 7.3, HCl/NaOH adj.) and NaOH (1 M) and passed over 100 mg CM resin (Waters *Accell* Plus *CM* weak cation exchange resin) packed in a 4 mm inner diameter column with polyethylene frits in order to trap the ^{135}La. The CM resin had been prepped by sequential washing with 5 mL acetonitrile, 5 mL 0.1 M HCl, 10 mL water, and 3 mL 1 M HEPES pH 7.3. After trapping the ^{135}La, the resin was washed with 25 mL of water. Finally, the column was eluted with 1 mL 0.1 M HCl to obtain the purified ^{135}La.

Specific activity measurements

Analysis by ICP-OES (inductively coupled plasma optical emission spectroscopy) was performed on the samples to determine the non-radioactive, competitive metal content. The trace metals were quantified using a ThermoScientific iCAP 6000 Series instrument with iTeva software. The spectrometer was calibrated against standard solutions containing La, Ba, Cr, Mn, Co, Fe, Zn and Cu, which were prepared by dissolution and dilution of chloride salts of the tested metals in 0.3 M HCl. Samples for analysis were likewise diluted in 0.3 M HCl.

The effective molar activity was determined experimentally *via* titration of the purified ^{135}La with DTPA. DTPA solutions were prepared in water by serial dilution to make concentrations spanning 8-5000 nM. From these, 400 µL of each concentration was moved to an Eppendorf tube and buffered by addition of 100 µL of HEPES (1 M, pH = 7.4). The molar amount of DTPA used in the titration ranged 3.2-2000 pmol in 5 steps. To each of these Eppendorf tubes, 10 µL of 0.1 M HCl containing 3.5-4.5 MBq of ^{135}La was added bringing the final pH to ~7 measured on pH paper. The titrations were performed in duplicate for each separation (n = 3) with one reacting at room temperature and the other reacting at 70 °C. After 30 minutes, the reactions were analyzed by thin-layer chromatography (TLC) performed on aluminum-backed silica (Merck TLC silica gel 60 F254), eluted with 5% (w/v) ammonium acetate in a 1:1 mixture of methanol and water. In this system La-DTPA moves with the eluent, while un-chelated La^{3+} remained at the origin. TLC plates were analyzed by autoradiography on a Cyclone Plus Storage Phosphor Scanner (PerkinElmer) and data analysis was performed using OptiQuant software (PerkinElmer). The reaction showing the chelation ratio closest to 50% was used to determine the amount of DTPA needed to chelate 100% of the added activity and thus the effective specific activity.

X-ray and Auger emission spectra

The initial-vacancy distribution and the energy spectra of X-rays and Auger electrons following the decays of isolated ^{135}La atoms were calculated according to the methodology presented by Lee et al. [16]

with 10^5 Monte Carlo simulated decays. Both the condensed phase and isolated atom models were used for determining the cascade distributions.

Dosimetry

On a cellular scale, dosimetry was treated in two ways: first by use of MIRDCell, a formalism developed by MIRD (Medical Internal Radiation Dose) for calculation of cellular S-values [20,21]; and second by the COOLER code [22]. The S-value is defined as the absorbed dose in the target structure from a radioactive decay in the source structure, typically given in the unit Gy/(Bq·s) and denoted as S(Target←Source). Contributions to the nucleus from the nucleus, S(N←N), from the cytoplasm, S(N←Cy), and from the cell surface, S(N←CS), were separately determined. In this work, we performed MIRD-based calculations, totally within the MIRD framework by taking the individual electron branches (Table 2), evaluating them in MIRDCell, and then summing the doses over all emissions [20]. MIRDCell was also used to calculate the cellular dosimetry of ^{177}Lu and ^{90}Y. This gave the MIRD cellular S-values as proxies for the cellular dosimetry for all three isotopes (depending on the target size and source distribution). For the calculations we chose a cell radius of 7 µm and nucleus radius of 5 µm. This allowed comparison with the COOLER formalism (the COOLER V79 cell setting has radii of 7.1 and 5.2 µm, respectively). COOLER is a new cellular dosimetry approach that uses Monte-Carlo derived effective stopping powers (based on PARTRAC simulations [23]). This is in contrast to MIRDCell which uses Cole's electron ranges to derive an electron stopping power [22,24]. The Monte-Carlo derived stopping powers generally result in altered dose distributions, especially for electrons with energies in the range of 5-35 keV, coinciding with the important Auger branches of the lanthanides.

In order to predict how a heterogeneously targeted tumor of macroscopic dimensions would receive dose across many cell diameters, electron dose kernels were calculated in two different ways. First, by taking the full electron emission spectrum (including Augers, nuclear beta emissions, and conversion electrons [13,14,25]) and folding it with the range-versus-energy relationship from Cole. The dose-point kernel was calculated in MATLAB for ^{135}La, ^{177}Lu and ^{90}Y. The calculation was performed using a step-size of 0.2 µm. Second, the electron dose-point kernel of ^{135}La was also calculated using the COOLER formalism.

Results:

Cyclotron Production of ^{135}La from ^{nat}Ba

When pressing the barium into the target holder, it was important to move quickly to limit the exposure of the barium to air. Within the minimal (~1 minute) pressing time, a white film was observed to form over

the normally shiny barium. The pressed target appeared smooth, and likely had very limited surface area after pressing, as compared to the dendritic chunks. In most experiments, no discoloration or alteration of the target surface was observed after irradiation at a target current of 15 μA. Both aluminum (100 μm) and niobium (25 μm) were tested as front foil materials, and we did not observe any qualitative difference in target behavior between the two.

The end-of-saturation bombardment (EOSB) yields for the nuclides ($t_{1/2}$ > 3 h) produced during proton irradiation of ^{nat}Ba at 15.8 MeV (after degradation in the aluminum cover foil) are given in Table 1.

nuclide	**$t_{1/2}$ (h)**	**EOSB *measured* (MBq/μA)**
^{135}La	18.9	429
^{135m}Ba	28.8	4
^{133}La	3.9	29
* ^{132}La	4.6	5

Table 1: Thick target EOSB yields for proton irradiation of ^{nat}Ba. Only nuclides with $t_{½}$ > 3 h are listed. *) ^{132}La is produced both directly and via decay of the co-produced ^{132m}La isomer. The number presented here reflects the amount of ^{132}La produced in total after all ^{132m}La has decayed to the ground state. Half-lives were obtained from refs: [11,13,26].

Shorter irradiations produced a proportionately larger amount of the short-lived impurities. These short-lived impurities will, at longer irradiation times, approach saturation and constitute a smaller proportion of the total radioactivity. Therefore the radionuclidic purity of ^{135}La (with respect to the decay rate of the other lanthanum isotopes) increases with irradiation time as long as the ^{135m}Ba impurity is chemically removed.

Target dissolution and purification of ^{135}La on Accell Plus CM resin

Dissolution of the irradiated ^{nat}Ba was always rapid (3-5 min) in the HCl solution. The trapping efficiency of ^{135}La on the small column of CM resin was >99%. Several loading conditions were tested: with or without the 30 minute heating step, and both ammonium acetate and HEPES buffers were tested: each at pH 4 and 6. It was observed that the 30-minute heating at 70 °C greatly improved trapping. When omitting this step loading efficiencies of only 50% were observed. Additionally, by re-acidifying and heating any washed-through solution it was possible to retain all previously untrapped activity on a second column (further illustrating the importance of heating). When comparing the two buffers,

ammonium acetate and HEPES, it was found that HEPES at pH = 6 resulted in higher trapping efficiency. The 0.1 M hydrochloric acid elution (1 mL) was >99% efficient at releasing the ^{135}La.

Chemical purity and molar activity measurements

ICP-OES analysis revealed the concentration of metal contaminants in the final elution. Barium was still present at a concentration of 3.68 ± 0.09 µg/MBq. Cr, Mn and Fe were measured in concentrations of 1.64 ± 1.05 ng/MBq, 1.19 ± 0.81 ng/MBq and 1.57 ± 0.33 ng/MBq, respectively. Using the final barium concentration, the separation factor was 138 ± 36. In principle, the barium removal could also have been verified by the absence of coproduced ^{135m}Ba, as this isotope is not formed by the decay of ^{135}La. However, the sensitivity and specificity of the gamma spectroscopy was not sufficient to detect the remaining low level of barium.

The molar activity of ^{135}La determined by stable lanthanum assay on ICP-OES was over-optimistic for the expected labelling efficiency. This is because any other lanthanide, or similar hard metal ion impurity, could compete for labelling positions on vectors. Instead, the effective molar activity was assessed by thin-layer chromatography analysis of DTPA titrations. In all cases, a small amount (10-15%) of ^{135}La remained at the origin of the TLC sheet no matter how large the excess of DTPA. This was believed to be due to formation of an inert lanthanum complex in the labeling solution, but the exact nature of the immobile ^{135}La was not determined. Assuming 10% of the ^{135}La was thermodynamically unavailable, the DTPA titrations showed an effective molar activity of 70.4 ± 20.0 GBq/µmol.

X-ray and Auger emission spectra

The initial-vacancy distribution for ^{135}Ba following the electron capture (EC) and internal conversion (IC) processes was calculated, and as expected >99.9% of the initial vacancies created in atomic shells were due to EC. The resulting total K vacancy probability was 84.9% and the total L vacancy probability was 11.9%. Internal conversion and electron capture processes in higher shells constituted the remaining 3.2% of vacancies.

The calculated X-ray and Auger spectra following the decay of ^{135}La in the condensed-phase approximation are shown in figure 2. The Auger-cascade simulations give only a small difference in the resulting Auger branching ratios between the condensed-phase (with continuous filling of the outermost vacancies) and isolated-atom approximations. The dose-point kernels derived from the two approximations were found to slightly differ from each other only in the first 100 nm [27]. For the purpose of dosimetry and possible therapeutic use, the effect is negligible and the condensed phase spectra were used for dosimetry calculations.

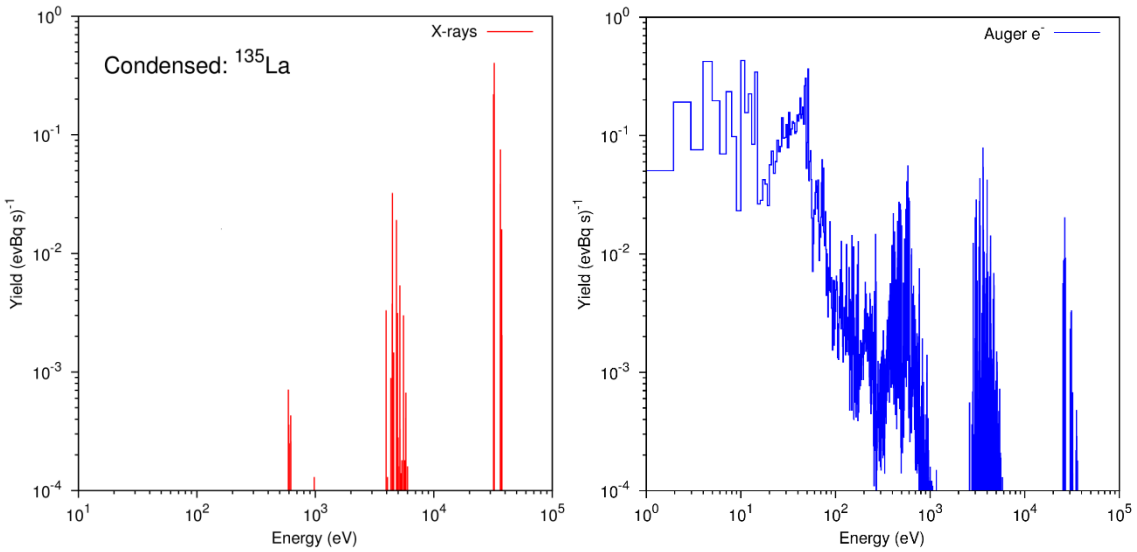

Figure 2 Histograms (bin-size 1 eV) showing the X-ray (red) and Auger (blue) kinetic energy spectra following the decay of ^{135}La atoms in the condensed-phase approximation of BrIccEmis. These results are tabulated in Table 2.

Yields per decay and mean energies of the main groups of Auger electrons are summarized in Table 2. The BrIccEmis derived spectrum is shown in Figure 2. Total energies released through X-rays and Auger electrons per decay, are 25.8 and 6.45 keV, respectively. There are on average 10.6 Auger electrons per decay (>97% of total) that have energies less than 4 keV. The maximum range of these very low-energy electrons is <0.5 μm in water [28].

	Yield /decay	Mean energy (keV)
Auger KLL	0.055	26.3

Auger KLX	0.025	31.0
Auger KXY	0.003	35.6
CK LLX	0.131	0.333
Auger LMM	0.580	3.53
Auger LMX	0.185	4.33
Auger LXY	0.014	5.15
CK MMX	0.634	0.104
Auger MXY	1.59	0.538
Super-CK NNN	0.277	0.007
CK NNX	1.33	0.049
Auger NXY	4.27	0.039
CK OOX	1.78	0.009
Auger OXY	0.023	0.030
Total	10.9	0.592

Table 2: Auger average spectrum following ^{135}La decay, the standard deviation in the total number of electrons ejected per decay is 3.2 e^-/(Bq s).

X-ray	Yield /decay	Mean energy (keV)
$K\alpha_1$	0.404	32.3
$K\alpha_2$	0.220	31.9
$K\beta_1$	0.075	36.5
$K\beta_2$	0.024	37.4
$K\beta_3$	0.039	36.4
$K\beta_4$	<0.001	37.5
$K\beta_5$	<0.001	36.8
KO*	0.003	37.6
L	0.098	4.71
M	0.007	0.711
N	<0.001	0.123
Total	0.871	29.6

*All other K X-rays.

Table 3. X-ray average spectrum following ^{135}La decay.

Dosimetry

The S-factors derived in this work are given in Table 4. From these results, it is clear that the calculated cellular S-factors based on the BrIccEmis derived Auger spectrum of ^{135}La are different from those obtained when using the spectrum from NuDat 2 [14]. The BrIccEmis derived spectrum yields higher S(N←N) but lower S(N←Cy) and S(N←CS). These changes follow from the fact that the BrIccEmis derived spectrum has a higher overall yield of low-energy Auger electrons and a slightly lower overall yield of the higher-energy K-shell Auger electrons. The low-energy emissions are more dose-intensive when inside the cell nucleus, while the higher energy emissions are more effective at supplying dose to the nucleus when they are localized in cytoplasm and on cell surfaces. This is because low energy emissions have a lower probability of reaching the nucleus from these compartments.

The S-factors calculated using the COOLER formalism show increased dose for the compartments (N←Cy) and (N←CS), 38% and 89% respectively while (N←N) showed a 5% decrease, using this newly calculated spectrum as compared to the MIRDCell formalism.

Comparing the dose delivered from ^{135}La to that of ^{177}Lu and ^{90}Y, it is seen that for (N←N), ^{135}La delivers a higher dose to the nucleus than ^{177}Lu and ^{90}Y. However, this is not the case when the decay occurs in the cytoplasm or on the cell surface. Comparing the new ^{135}La spectrum to ^{177}Lu, the dose ratio is 4 and 5.5 for the compartments (N←Cy) and (N←CS) respectively. This means that four disintegrations of ^{135}La are needed to deliver absorbed dose, equal to that associated with a single disintegration of ^{177}Lu in the cytoplasm. For ^{90}Y the dose ratios are 1.3 and 2, respectively. However, the number of interest when assessing the potential of a therapeutic isotope is not the dose delivered per disintegration, but the target-to-normal ratio i.e., the dose delivered to the target divided by the dose delivered to normal tissue.

	MIRDCell		COOLER	
	^{135}La new spectrum	^{135}La NuDat 2 spectrum	^{135}La new spectrum	^{135}La NuDat 2 spectrum
N←N	1.29E-03	9.51E-04	1.23E-03	9.45E-04
N←Cy	6.81E-05	7.06E-05	9.39E-05	1.02E-04
N←CS	3.09E-05	3.46E-05	5.84E-05	6.41E-05

Table 4: Comparison of the cellular S-factors [Gy/(Bq*s)] for ^{135}La calculated in MIRDCell (left) and COOLER (right) using the new Monte Carlo based Auger spectrum and, as reference, the input spectrum available in the NuDat 2 database [14].

COOLER	MIRDCell

^{135}La new spectrum	^{177}Lu MIRD spectrum	^{90}Y MIRD spectrum
1.23E-03	1.05E-03	2.54E-04
9.39E-05	2.78E-04	9.09E-05
5.84E-05	1.72E-04	6.15E-05

Table 5 A comparison of the cellular S-factor [Gy/(Bq*s)] of ^{135}La calculated in COOLER, to those of the traditional β-emitting therapeutic radionuclides ^{177}Lu and ^{90}Y calculated in MIRDCell.

The relative merit of ^{135}La for single cell or small cell-cluster therapy as compared with the "standard" therapeutic nuclides ^{177}Lu and ^{90}Y is obvious in Figure 3. It shows the fraction of emitted electron energy absorbed within spheres of ever growing radii. Only ^{135}La is treated using both the COOLER and the Cole stopping power approach, seeing that the COOLER formalism, at present, is not capable of handling the high electron energies associated with ^{177}Lu and ^{90}Y decay.

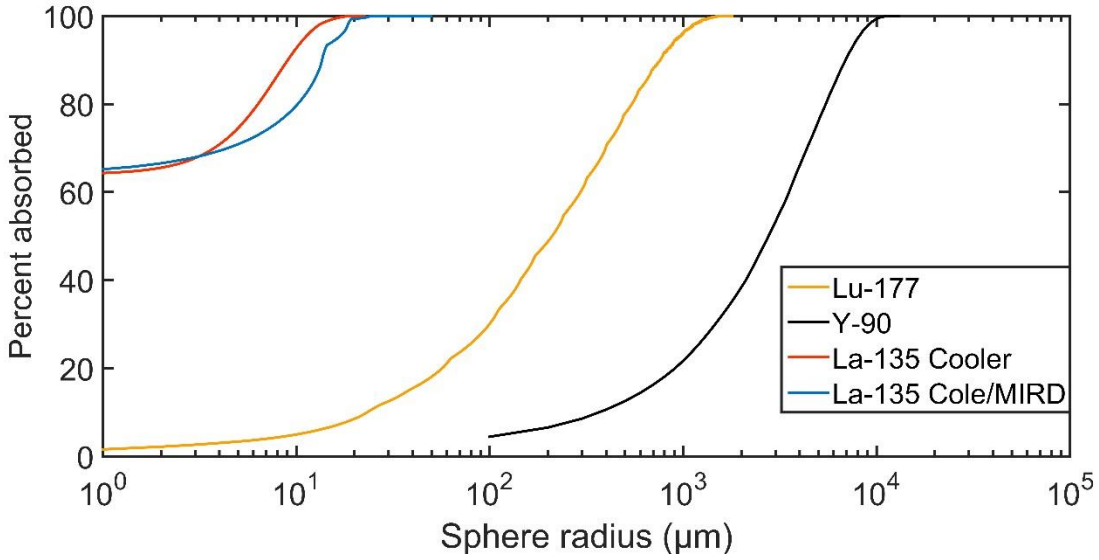

Figure 3 Fraction of electron kinetic energy absorbed within spheres as function of sphere radius. The energy deposition is calculated using the Cole stopping power as stated and used in the introduction of MIRD Cellular S-values [24], with exception of the "La-135 Cooler" curve (red) which was calculated using the COOLER code. The input for the continuous beta spectra are taken from RADAR[29] (^{90}Y and ^{177}Lu), the conversion- and Auger electrons from NuDat 2, except for ^{135}La, where the new, calculated Auger spectrum is used. Photons, including bremsstrahlung, are omitted.

Figure 3 however, hides the full impact of the Auger emissions from ^{135}La. In very small spheres (radius less than the diameter of cell nucleus) surrounding a ^{135}La decay, the local dose is very high. This can be seen in Figure 4 which shows the dose-point kernel for ^{135}La as calculated with the new spectrum and both the COOLER and the Cole stopping power formalisms.

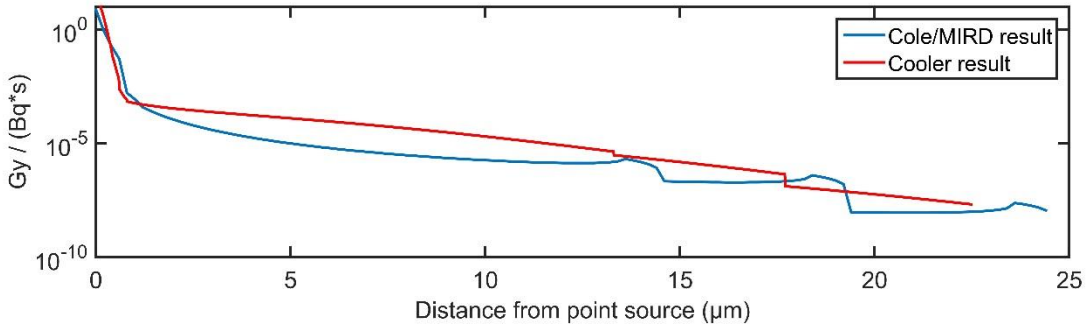

Figure 4: Dose-point kernels for ^{135}La Auger electron emissions (X-rays are not included) for both the COOLER and Cole/MIRD methodologies. In both cases, the calculations were performed using the Auger spectrum obtained from the BrIccEmis simulation.

Discussion:

The Auger emitter ^{135}La is a potential radionuclide for targeted internal therapy. From the view of production and purification, the route via proton irradiation of ^{nat}Ba is straightforward. Clearly, the rate of production and the radionuclidic purity of ^{135}La could be improved by irradiating enriched ^{135}Ba, but further target development would be required to allow either irradiation of a barium oxide or salt, or to accommodate reduction of recycled $^{135}Ba^{2+}$ after the separation procedure. While the overall separation factor achieved in this report is not impressive ~10^2, the fact that high labeling effective specific activity is obtained demonstrates that rigorous separation is not critical. Here, the measured effective specific activity is a positive indicator for the expected labeling yield. The value measured by DTPA titration of (70.4 ± 20.0 GBq/μmol) corresponds well with what would be expected from the ICP analysis. If, for some applications, higher effective specific activities are required, an additional step to ensure the removal of iron and manganese could be employed [30]. It should be noted that the exact impurity profile of competing metals will depend on the initial purity of the barium stock used.

When turning to the emissions of ^{135}La, we show the results of calculations using the BrIccEmis code from Lee et al. [16]. Importantly this method accounts for multiple vacancies during the cascade. Notably, if the atomic transition energies are approximated using neutral binding energies, and thereby neglecting the effect of multiple vacancies, this could give rise to multiple energies for a given atomic transition due to the stochastic nature of the Auger cascade. Falzone & Lee et al. showed that MIRD RADTABS disagree with the experimental L-Auger spectrum of ^{131}Cs and demonstrated that the theoretical L-Auger energy spectrum of ^{131}Cs agreed with experiment only when the effect of multiple vacancies was taken into account [27,31] .

In the present case, the use of the newly calculated Auger spectrum does not result in dramatically different cellular dosimetry. However, the exact shape of the spectrum at low energies can become extremely important as cellular and subcellular targeting becomes more exact. This is because the expected biological effect of Auger emitters may not solely rely on the dose, but also on the RBE of the low energy electrons. An important part of the Auger emitter concept is the expectation of an RBE larger than that of conventional gamma or beta irradiation. RBE is the measure used to compare different types of radiation gray-to-gray, assessing the biological damage done. A common measure for the biological damage is DNA double-strand breaks, which are potentially more likely to occur in close proximity to the decay site of an Auger emitter. For higher energy electron and beta emissions (> 20 keV), creating a double-strand break with a single pass of an electron is highly unlikely because the mean path length between subsequent ionization events is much larger than the distance between the DNA strands. Therefore multiple electrons stemming from multiple decays have to pass through or get in close proximity to the same area of the DNA strand to create a double-strand break. With an Auger emitter this is not the case. Due to the multiple electrons emitted in a single decay (10.9 ± 3.2/decay for ^{135}La) only a single decay is potentially enough to cause the double-strand break if the decay occurs close to the DNA. Additionally, the decaying atom would find itself highly ionized due to multiple emissions of Auger electrons and thus could be highly oxidizing to the immediate environment. From a physical perspective, these two factors combined should result in an RBE much higher than 1, meaning more effective therapy per gray deposited. A recent paper has described how the cell surface is more radiosensitive than assumed in MIRD [32]. The calculations presented in this paper only consider dose to the nucleus, however incorporating the cell surface as a sensitive target would make the case for ^{135}La even stronger, seeing that this would decrease the importance of internalization.

It is also important to understand that the low amount energy emitted per decay of ^{135}La does not preclude effective therapy. For therapeutic benefit, the relevant metric is not the absolute dose-per-decay but the ratio of the dose absorbed by the target to the dose absorbed by the surrounding healthy tissue. Commonly, the limiting factor is the absorbed dose in healthy tissue immediately surrounding the targeted cell, or the absorbed dose in clearance organs. When considering the absorbed dose to the immediate surroundings, the benefit of using ^{135}La is clear from Figure 3 and Figure 4, where the absence of higher energy beta electrons and the limited Auger-electron range of ^{135}La results in dramatically reduced dose beyond one cell diameter. As is the case with any Auger emitter, there are clear benefits of using ^{135}La when the target being treated is very small.

Conclusion:

A method has been developed allowing the production of clinically relevant amounts of ^{135}La using medical cyclotrons. The developed purification method is fast, robust and essentially loss-less. ^{135}La has a well-suited half-life for therapy. The calculated cellular dosimetry shows that the emissions from ^{135}La lead to cellular S-values that are promising for internal radionuclide therapy of very small targets, with dosimetry superior to ^{177}Lu and ^{90}Y at single-cell dimension. This along with the mounting evidence of Auger emitters having an RBE > 1 strongly motivates further research in application of Auger emitters in treatment of single cancerous cells and micro-metastasis.

Acknowledgements:

This work was supported by the European Union Seventh Framework Programme FP7/2007-2013 under Grant 602820 (Mathias), and by the Australian Research Council Discovery Grant DP14 0103317.

References

[1] Pfeifer AK, Gregersen T, Grønbæk H, Hansen CP, Müller-Brand J, Herskind Bruun K, et al. Peptide receptor radionuclide therapy with 90Y-DOTATOC and 177Lu-DOTATOC in advanced neuroendocrine tumors: Results from a Danish cohort treated in Switzerland. Neuroendocrinology 2011;93:189–96. doi:10.1159/000324096.

[2] de Jong M. Combination Radionuclide Therapy Using 177Lu- and 90Y-Labeled Somatostatin Analogs. J Nucl Med 2005;46:13–7.

[3] Müller C, Reber J, Haller S, Dorrer H, Köster U, Johnston K, et al. Folate receptor targeted alpha-therapy using terbium-149. Pharmaceuticals 2014;7:353–65. doi:10.3390/ph7030353.

[4] Müller C, Reber J, Haller S, Dorrer H, Bernhardt P, Zhernosekov K, et al. Direct in vitro and in vivo comparison of 161Tb and 177Lu using a tumour-targeting folate conjugate. Eur J Nucl Med Mol Imaging 2014;41:476–85. doi:10.1007/s00259-013-2563-z.

[5] Müller C, Zhernosekov K, Köster U, Johnston K, Dorrer H, Hohn A, et al. A unique matched quadruplet of terbium radioisotopes for PET and SPECT and for α- and β- radionuclide therapy: an in vivo proof-of-concept study with a new receptor-targeted folate derivative. J Nucl Med 2012;53:1951–9. doi:10.2967/jnumed.112.107540.

[6] Grünberg J, Lindenblatt D, Dorrer H, Cohrs S, Zhernosekov K, Köster U, et al. Anti-L1CAM radioimmunotherapy is more effective with the radiolanthanide terbium-161 compared to lutetium-177 in an ovarian cancer model. Eur J Nucl Med Mol Imaging 2014;41:1907–15.

doi:10.1007/s00259-014-2798-3.

[7] Kassis AI. Molecular and cellular radiobiological effects of Auger emitting radionuclides. Radiat Prot Dosimetry 2011;143:241–7. doi:10.1093/rpd/ncq385.

[8] Howell RW, Kassis AI, Adelstein SJ, Rao D V, Wright HA, Hamm RN, et al. Radiotoxicity of platinum-195m-labeled trans-platinum (II) in mammalian cells. Radiat Res 1994;140:55–62. doi:10.2307/3578568.

[9] Azure MT, Sastry KSR, Archer RD, Howell RW, Rao D V. Microscale Synthesis of Carboplatin Labels with the Auger Emitter Platinum-193m: Radiotoxicity Versus Chemotoxicity og the Antitumor Drug in Mammalian Cells. AAPM Symp. Ser. No.8, 1992.

[10] Kassis AI. Cancer therapy with Auger electrons: are we almost there? J Nucl Med 2003;44:1479–81.

[11] Abel EP, Clause HK, Fonslet J, Nickles RJ, Severin GW. The Half-lives of 132La and 135La. arXiv.org 2017:1–11.

[12] Fonslet J, Tran T, Quan-Lee B, Severin G. 135La for Auger-based therapy: preparation, imaging and emissions. J Label Compd Radiopharm 2015;58:S24.

[13] Singh B, Rodionov AA, Khazov YL. Nuclear Data Sheets for A = 135. Nucl Data Sheets 2008;109:517–698. doi:10.1016/j.nds.2008.02.001.

[14] Nudat 2 n.d. http://www.nndc.bnl.gov/nudat2/ (accessed May 30, 2017).

[15] Lee BQ, Kibédi T, Stuchbery E, Robertson K. Atomic radiations in the decay of medical radioisotopes: a physics perspective. Comput Math Methods Med 2012;2012:651475. doi:10.1155/2012/651475.

[16] Lee BQ, Nikjoo H, Ekman J, Jönsson P, Stuchbery AE, Kibédi T. A stochastic cascade model for Auger-electron emitting radionuclides. Int J Radiat Biol 2016;92:641–53. doi:10.3109/09553002.2016.1153810.

[17] Prescher K, Peiffer F, Stueck R, Michel R, Bodemann R, Rao MN, et al. Thin-target cross sections of proton-induced reactions on barium and solar cosmic ray production rates of xenon-isotopes in lunar surface materials. Nucl Inst Methods Phys Res B 1991;53:105–21. doi:10.1016/0168-583X(91)95645-T.

[18] Tárkányi F, Ditrói F, Király B, Takács S, Hermanne A, Yamazaki H, et al. Study of activation cross sections of proton induced reactions on barium: Production of 131Ba 131Cs. Appl Radiat Isot 2010;68:1869–77. doi:10.1016/j.apradiso.2010.03.010.

[19] Severin GW, Gagnon K, Engle JW, Valdovinos HF, Barnhart TE, Nickles RJ. 44gSc from metal calcium targets for PET. AIP Conf Proc 2012;1509:125–8. doi:10.1063/1.4773953.

[20] Vaziri B, Wu H, Dhawan AP, Du P, Howell RW. MIRD pamphlet No. 25: MIRDcell V2.0 software tool for dosimetric analysis of biologic response of multicellular populations. J Nucl Med 2014;55:1557–64. doi:10.2967/jnumed.113.131037.

[21] Goddu SM, Howell RW, Rao D V. Cellular dosimetry: absorbed fractions for monoenergetic electron and alpha particle sources and S-values for radionuclides uniformly distributed in different cell compartments. J Nucl Med 1994;35:303–16.

[22] Siragusa M, Baiocco G, Fredericia PM, Friedland W, Groesser T, Ottolenghi A, et al. The COOLER Code: A Novel Analytical Approach to Calculate Subcellular Energy Deposition by Internal Electron Emitters. Radiat Res 2017;188:204–20. doi:10.1667/RR14683.1.

[23] Friedland W, Dingfelder M, Kundrát P, Jacob P. Track structures, DNA targets and radiation effects in the biophysical Monte Carlo simulation code PARTRAC. Mutat Res - Fundam Mol Mech Mutagen 2011;711:28–40. doi:10.1016/j.mrfmmm.2011.01.003.

[24] Cole A. Absorption of 20-eV to 50,000-eV Electron Beams in Air and Plastic. Radiat Res 1969;38:7. doi:10.2307/3572707.

[25] Lee BQ, Kibédi T, Stuchbery AE. Auger yield calculations for medical radioisotopes. EPJ Web Conf 2015;91:7. doi:10.1051/epjconf/20159100007.

[26] Khazov Y, Rodionov A, Kondev FG. Nuclear Data Sheets for A = 133. Nucl Data Sheets 2011;112:855–1113. doi:10.1016/j.nds.2011.03.001.

[27] Falzone N, Lee BQ, Fernandez-Varea JM, Kartsonaki C, Stuchbery AE, Kibedi T, et al. Absorbed dose evaluation of Auger electron-emitting radionuclides: impact of input decay spectra on dose point kernels and S -values. Phys Med Biol 2017;62:2239–53. doi:10.1088/1361-6560/aa5aa4.

[28] Emfietzoglou D, Nikjoo H. Accurate electron inelastic cross sections and stopping powers for liquid water over the 0.1-10 keV range based on an improved dielectric description of the Bethe surface. Radiat Res 2007;167:110–20. doi:10.1667/RR0551.1.

[29] RADAR Home n.d. http://www.doseinfo-radar.com/RADARHome.html (accessed May 30, 2017).

[30] Fonslet J, Tietze S, Jensen AI, Graves SA, Severin GW. Optimized procedures for manganese-52: Production, separation and radiolabeling. Appl Radiat Isot 2017;121:38–43. doi:10.1016/j.apradiso.2016.11.021.

[31] Eckerman KF, Endo A. MIRD: radionuclide date and decay schemes. Society of Nuclear

Medicine; 2008.

[32] Paillas S, Ladjohounlou R, Lozza C, Pichard A, Boudousq V, Jarlier M, et al. Localized Irradiation of Cell Membrane by Auger Electrons Is Cytotoxic Through Oxidative Stress-Mediated Nontargeted Effects. Antioxid Redox Signal 2016;25:467–84. doi:10.1089/ars.2015.6309.